



ELSEVIER

Optics and Lasers in Engineering 35 (2001) 135–147

OPTICS and LASERS
in
ENGINEERING

The application of optical coherence tomography to problems in polymer matrix composites

Joy P. Dunkers^{a,*}, Frederick R. Phelan^a, Daniel P. Sanders^a,
Matthew J. Everett^b, William H. Green^c, Donald L. Hunston^a,
Richard S. Parnas^a

^a*Polymer Composites Group, National Institute of Standards and Technology, Gaithersburg, MD 20899, USA*

^b*Medical Technology Program, Livermore National Laboratory, Livermore, CA, USA*

^c*Weapons and Materials Research Directorate, U.S. Army Research Laboratory, Aberdeen Proving Ground, MD, USA*

Received 3 November 2000; accepted 23 January 2001

Abstract

The Composites Group at the National Institute of Standards and Technology has found optical coherence tomography (OCT) to be a powerful tool for non-destructive characterization of polymer matrix composites. Composites often exhibit superior properties to traditional materials such as wood and metal. However, the barrier to their widespread infiltration into consumer markets is cost. Composites can be made more cost competitive by improved composite design, process optimization, and quality control. OCT provides a means of evaluating the three aforementioned areas. OCT is a very versatile technique that can be applied to a variety of problems in polymer composites such as: microstructure determination for permeability and mechanical property prediction, void, dry spot, and defect detection, and damage evaluation. Briefly, OCT uses a low coherence source such as a superluminescent diode laser with a fiber optic based Michelson interferometer. In this configuration, the composite is the fixed arm of the interferometer. Reflections from heterogeneities within the sample are mapped as a function of thickness for any one position. Volume information is generated by translating the sample on a motorized stage. Information about the location and size of a feature within the composite is obtained. In this work, the power of OCT for imaging composite microstructure and damage is presented. An example of permeability prediction using the composite microstructure imaged from OCT is demonstrated. The effect of image processing on the value of permeability is discussed. Using the same sample, OCT imaging of composite impact damage is

* Corresponding author. Tel.: + 1-301-975-6841; fax: + 1-301-975-4932.

E-mail address: joy.dunkers@nist.gov (J.P. Dunkers).

compared to more traditional techniques, X-ray computed tomography and confocal microscopy. Published by Elsevier Science Ltd.

Keywords: Optical coherence tomography; Composites; Microstructure; Permeability; Damage; Imaging

1. Introduction

In the past, microstructure and damage in polymer matrix composites have often been characterized using destructive techniques such as microscopy on sectioned samples which provides detailed information on a small size scale. The capability to measure these features non-destructively, however, is very desirable since that permits monitoring of damage evolution and correlation of the results with microstructural features that can initiate, influence, or even control the damage. It is even more advantageous if these measurements are performed with a single technique because this eliminates the complications involved in combining data from different sources. Optical coherence tomography (OCT) is a measurement method that can characterize both microstructure and damage with high resolution and good penetration depth.

OCT is a non-invasive, non-contact optical imaging technique that allows the visualization of microstructure within scattering media [1–3]. OCT uses light in a manner analogous to the way ultrasound imaging uses sound, providing significantly higher spatial resolution (10–20 μm) albeit with shallower penetration depth. OCT is based upon low-coherence optical ranging techniques where the optical distance to individual sites within the sample is determined by the difference in time, relative to a reference light beam, for an incident light beam to penetrate and backscatter within the sample. This temporal delay is probed using a fiber optic interferometer and a broadband laser light source. The fiber optic interferometer consists of single-mode optical fiber coupled with a 50/50 fiber optic splitter that illuminates both the sample and a linearly translating reference mirror. Light reflected from the reference mirror recombines with light back-scattered and reflected from the sample at the 50/50 splitter to create a temporal interference pattern which is measured with a photodiode detector. The resulting interference patterns are present only when the optical path difference of the reference arm matches that of the sample arm to within the coherence length of the source. The incident light beam is scanned and repeated measurements are performed at different transverse positions to generate a two-dimensional array which represents the backscattering or backreflection of a cross-sectional plane of the material. This data can be displayed as a gray scale or false color image.

The axial, or z , spatial resolution that can be obtained with OCT is determined by the coherence length, or inverse spectral width, of the light source and is typically 10–20 μm (Fig. 1). The light source is typically a superluminescent diode laser, with a resolution as low as 10–15 μm . Femtosecond laser sources have also been used to achieve higher resolutions of $< 5 \mu\text{m}$ and imaging speeds of several frames per second [4,5]. The transverse, or x , spatial resolution of OCT is determined by the focal spot

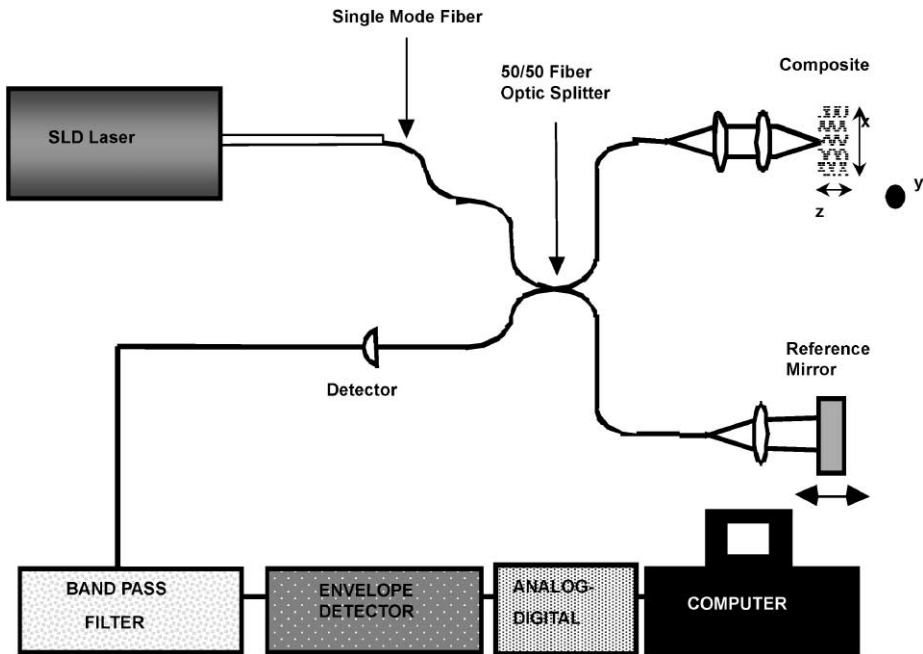


Fig. 1. Schematic representation of the solid state laser and OCT system layout.

size on the sample, which is typically 10–30 μm . The ultimate limitation on the depth of penetration within the sample is the attenuation of light caused by scattering. Depth of penetration is practically 5 mm–1 cm for composites. Three-dimensional images of the sample are obtained by rastering the sample in the x direction between successive OCT measurements along the y -axis.

Knowledge of the permeability tensor in liquid composite molding (LCM) is important for process optimization. The permeability tensor dictates the speed and direction of the resin, and its determination is critical for successful mold filling. Currently, the most reliable and commonly used technique for obtaining permeability values is via experimental measurements in either radial or uni-directional flow configurations [6]. However, experimental characterization is slow, as it involves a large number of carefully controlled experiments over a large range of volume fractions. Another more serious limitation is that it is difficult to conduct experiments on the materials in the deformed states they encounter when placed in LCM tooling, although there have been some recent efforts [7].

In light of these limitations, computational prediction of permeability [8–12] offers a potentially accurate and robust alternative to experimental methods. Such calculations typically involve imposing a pressure drop across the media, solving the appropriate transport equations for the detailed flow field, and then back-calculating the permeability by applying Darcy's law. The biggest drawback of this approach has been the inability to accurately determine the detailed geometry of the fibrous preform

materials, which in addition to many intricate structural features, typically contain statistical variations and defects in their microstructure [13]. Without a precise representation of the media, it is not possible to accurately predict permeability values using computational methods.

There have been two main approaches to the problem of microstructure determination. The first is to perform calculations on small, computationally efficient “unit cell” structures using nominal dimensions that represent the average preform weave structure. The major problem with this approach is that calculations on the “average” unit cell structure do not in general, yield an accurate value for the average permeability [13]. A second approach is to determine the microstructure via optical methods (e.g., microscopy), and directly perform the numerical calculation on a discretization of the optical image. This approach has the advantage of accurately representing the media, and by including large sections of the media in the image, variations and defects in the microstructure are automatically accounted for in the calculation. However, until recently, this approach was probably even more tedious to perform than direct experimental measurement of permeability since the composite specimens typically had to be carefully sectioned, polished, and examined. However, OCT offers a means for rapidly and non-destructively determining the microstructure of fiber reinforced plastic materials, potentially leading to a robust means of computational permeability prediction.

OCT as a non-destructive evaluation (NDE) tool compares very favorably to more established composite NDE techniques. Both transducer and laser based ultrasonics have been used for NDE of polymer composites. Their practical resolution is on the order of 1 mm with tens of millimeters in penetration depth [14,15]. A major drawback to ultrasonics is that the depth of a feature must be determined by model studies, whereas, it is known precisely using OCT. However, ultrasonic testing can evaluate carbon fiber composites, which OCT cannot since it is an optical technique. Both OCT and ultrasonics suffer from contrast degradation and shadowing through the sample thickness. Two X-ray based techniques have been studied. X-ray radiometry has a spatial resolution of hundreds of microns and tens of millimeters in penetration depth [16]. The main drawback in performing X-ray radiometry is that a dye penetrant must be used for contrast. A method more recently applied to composites, micro-focus X-ray computed tomography (CT) has a resolution on the order of tens of microns and penetration similar to its counterpart. However, several inches to well over a foot of polymer composite can be penetrated and completely imaged using sources in the energy range 160–450 keV. The accuracy of the X-ray attenuation measurement, and thereby the feature intensity and position, is a complex function of many variables and additional constraints may, but not necessarily, complicate image interpretation. It is important to note that with the energies typically used for X-ray CT, damage in the material must have separation equal to or greater than the spatial resolution to be detected [17].

Laser scanning confocal microscopy (LSCM) has been used extensively in the biomedical arena. Scanning confocal microscopy utilizes variable pinholes to reject the out-of-focus image. The wavelength, numerical aperture of the objective, and size of the pinhole dictates the resolution in the thickness or axial direction. The thickness

resolution of OCT is solely determined by the bandwidth of the source and the numerical aperture of the focusing objective. For the same optical configuration, OCT has been shown to have substantially higher signal-to-noise and narrower point spread function than confocal microscopy [18]. Using OCT, the sample can be probed deeper with more image detail. OCT does not have an advantage over LSCM for imaging features close to the surface [18]. OCT is only performed in reflection mode while LSCM is amenable to either reflection or transmission. Also, sample birefringence can confound standard OCT images but does not pose an issue for LSCM. When considering NDE techniques for microstructure evaluation, OCT offers an excellent combination of spatial resolution, depth of field, and imaging accuracy.

In this work, the potential of OCT for imaging both microstructure and damage is demonstrated. OCT was used to determine the actual microstructure for permeability prediction. The volumetric, grayscale OCT images were converted to binary images using custom written software. Then, these images were input into a 3D flow code based on a lattice Boltzmann formulation for prediction of axial and transverse permeabilities and compared to experimental values. The predicted permeabilities compare well with the experimental axial and transverse values. The effect of image processing on the computed flow velocity and consequently the permeability is discussed. OCT imaging of composite damage is shown by a tomographic reconstruction and re-slicing of impact damage along the thickness of the composite. This re-slicing of the image data reveals the progression of cracking and delamination within the composite. The OCT images are compared to images from confocal microscopy and X-ray CT on the same sample.

2. Experimental

2.1. Materials

The epoxy resin system consisted of a diglycidyl ether of bisphenol A (DGEBA) monomer (Tactix123, Dow Chemical Company, Midland, MI) and two amines.¹ Aromatic methylene dianiline (MDA) and aliphatic poly(propylene glycol)bis(2-aminopropyl ether) (Jeffamine D400) ($M_{r,n} \approx 400$) were purchased and used as received from Aldrich (Minneapolis, MN). The oxirane/amine stoichiometry was 2 mol oxirane/1 mol amine. The amine composition consisted of 0.07 mol MDA and 0.93 mol D400. Details of the mixing and resin transfer molding are provided elsewhere [19]. The refractive index of the postcured resin and of the fibers is 1.552 ± 0.004 and 1.554 ± 0.004 , respectively, as measured by white light and index matching fluids. The fiber volume fraction is 44%. To generate the damage, the composite was secured in a vice and impacted with a blunt object at various places with various loads.

¹ Identification of a commercial product is made only to facilitate experimental reproducibility and to adequately describe experimental procedure. In no case does it imply endorsement by NIST or imply that it is necessarily the best product for the experimental procedure.

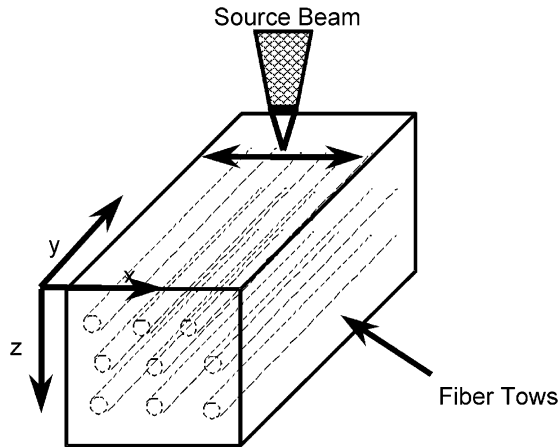


Fig. 2. Schematic showing the SLD source orientation and sampling directions with respect to the composite.

2.2. Instrumentation

The imaging system used in this study is schematically shown in Fig. 1. A commercial superluminescent Diode (SLD) source (AFC Technologies Inc., Hull, Quebec, Canada) was used for the work reported here. The source operated at $1.3\ \mu\text{m}$ with an output power of up to $8\ \text{mW}$ and a spectral bandwidth of $70\ \text{nm}$, corresponding to a theoretical axial spatial resolution of $\approx 11\ \mu\text{m}$. The light was coupled into a single-mode fiber-optic Michelson interferometer and delivered to both the reference mirror and the sample. The reference mirror was mounted after a scanning retroreflector. Transverse scanning was performed using a computer controlled motorized stage to translate the sample, as shown in Fig. 2.

The interferometric signal was electronically filtered with a bandpass centered on the fringe or heterodyne frequency. The filtered fringe waveform was then demodulated, digitized and stored on a computer. The high dynamic range of this system allowed back-reflections as weak as femtowatts of power to be detected. Images were displayed by mapping the logarithm of the signal strength to a gray scale look-up table. The acquisition time for each image was approximately 1 min. The axial (z) measurement range was determined by the distance the reference mirror moves ($7\ \text{mm}$) normalized by the refractive index (n) of the sample: $7\ \text{mm}/n$. The probe beam was focused to a $30\ \mu\text{m}$ diameter spot at a depth of approximately $750\text{--}1000\ \mu\text{m}$ below the surface of the sample.

A Zeiss laser scanning confocal microscope was used in reflection at $543\ \text{nm}$ at $5\ \text{mW}$ with a pinhole diameter of $99\ \mu\text{m}$. The confocal images are a collage of 12 individual, 12 bit images collected with a $10\times/0.3$ objective. The individual images consist of a 512×512 area of pixels. The image collage represents an area of about $2\ \text{mm}$ along the x -axis and $1.9\ \text{mm}$ along the y -axis. The axial resolution is $15\ \mu\text{m}$.

The sample was inspected using a customized ACTIS 600/420 X-ray CT system designed and constructed by Bio-Imaging Research, Inc., and installed at the U.S. Army Research Laboratory (ARL) at Aberdeen Proving Ground, Maryland. The system was designed to meet ARL performance specifications. A dedicated embedded industrial computer system controls data collection and image reconstruction, viewing, and processing. A 5 mm long section of the sample (y -axis) was scanned in rotate only mode using the 160 keV microfocus tube and the image intensifier. The sample was scanned over the area with visible indications of impact damage. The cross-sectional image is collected on the x - z plane. The slice thickness and slice increment were 100 μm , resulting in contiguous scans. Scan time was about 1.5 min/slice with 51 slices required to scan the 5 mm section. Each slice was reconstructed to a 512 by 512 image matrix using 5120 views. The tube energy and current used were 160 keV and 0.025 mA, respectively, and the focal spot was 10 μm .

3. Results and discussion

An example of the utility of microstructural information gathered using OCT is discussed below using images for prediction of reinforcement permeability. The reinforcement is an unidirectional E-glass fabric and is idealized in Fig. 2. First, OCT was compared to optical microscopy to evaluate how well OCT represents the actual microstructure. The results are discussed in previous work [20], and we have concluded that OCT does accurately image the microstructure at the desired size scale for permeability prediction. The permeability values discussed in this work were calculated from grayscale OCT images that were processed to binary images and input

Table 1
Experimental and predicted values for axial (K_{ax}) and transverse (K_{tr}) permeability and Brinkman fraction

| Sample name | Type of processing | Image set | Axial $K \times 10^{-4}$ (mm^2) | Transverse $K \times 10^{-4}$ (mm^2) | Anisotropy ratio | Brinkman fraction |
|--------------|--------------------------|-----------|--|---|------------------|-------------------|
| Experimental | N/A | N/A | 5.3 ± 2.6 | 0.750 | 7.0 | 0.770 |
| Data 1 | Manual | 87–91 | 4.45 | 0.882 | 5.06 | 0.767 |
| Data 2 | Manual | 75–95 | 3.81 | 0.992 | 4.11 | 0.788 ± 0.021 |
| Data 3 | Automated no smoothing | 75–95 | 2.83 | 0.654 | 4.32 | 0.768 ± 0.021 |
| Data 4 | Automated smoothing | 75–95 | 3.18 | 0.991 | 3.21 | 0.750 ± 0.027 |
| Data 5 | Automated smoothing | 4–24 | 5.09 | 0.934 | 5.45 | 0.727 ± 0.014 |
| Data 6 | Manual roughened | 75–95 | 2.73 | 0.662 | 4.12 | 0.795 ± 0.021 |
| Data 7 | Manual dilated | 75–95 | 2.99 | 0.767 | 3.90 | 0.837 ± 0.020 |
| Data 8 | Automated post-processed | 75–95 | 3.27 | 0.878 | 3.72 | 0.768 ± 0.014 |

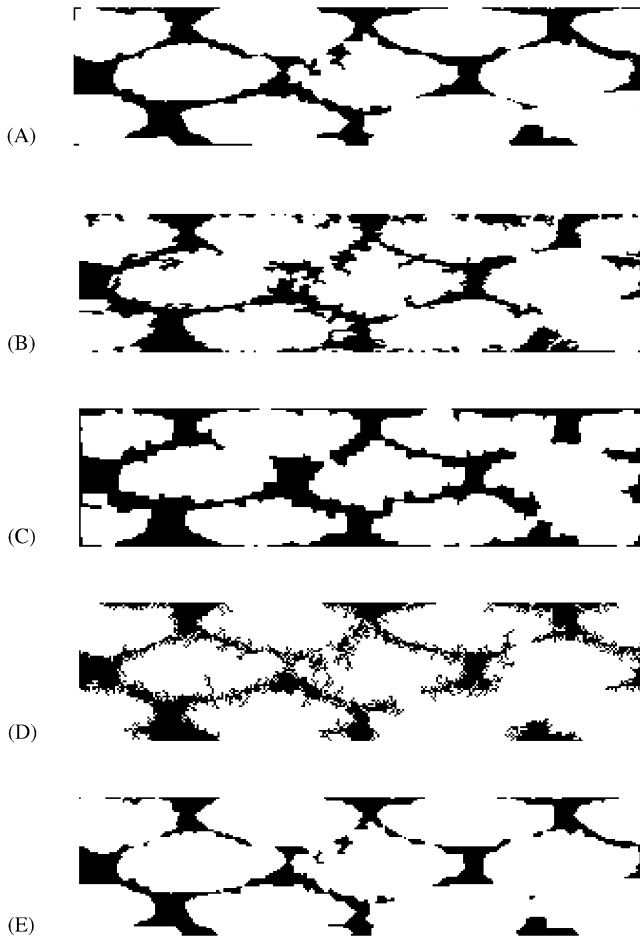


Fig. 3. Binary images resulting from different image processing techniques. Manually processed image (A), automatically processed image (B), automatically processed image with smoothing (C), manually processed image in A with added random roughness (D), manually processed image in A with topological dilation (E).

into a lattice-Boltzmann micro-flow code [20]. It was found that the quality of the image processing had a large influence on the calculated permeability values. The experimental and calculated axial (K_{ax}) and transverse (K_{tr}) permeabilities are provided in Table 1 for comparison. K_{ax} describes flow along the y -axis and K_{tr} along the x -axis shown in Fig. 2. It should be noted that because of the large variation in reinforcement microstructure, permeability values for a single volume fraction can vary as much as 30%–50%. OCT image sets for computing K values within this table were processed in two different ways: For the “Manual” method, the top outlines were drawn by sight and filled in to generate a binary image. Images using the “Automated” method were processed as described in previous work [20]. Fig. 3 displays image number 75 from select data sets for visual comparison. For Data 2

(Fig. 3A), the K_{ax} of $3.81 \times 10^{-4} \text{ mm}^2$ is considered to be the best possible value because the images are manually drawn. The 21 images used in these calculations represent only a width of 6.0 mm, a depth of approximately 1.5 mm, and, most importantly, a length of 1.0 mm. For comparison, the size of the reinforcement used in experimental determination of permeability is 15 cm wide (x), 1.3 cm deep (z) and 15 cm long (y).

The Brinkman fraction (Table 1) is defined as the area occupied by the tows and varies slightly from image to image. The average Brinkman fraction is shown along with the standard deviation of the image set. The higher the area occupied by the tows (or the higher the Brinkman fraction), the lower K_{ax} and K_{tr} because there is less open space available for fluid flow. If the Brinkman fractions are considered, then the K_{ax} for Data 3 (Fig. 3B) should be higher than for Data 2 (Fig. 3A) since the Brinkman fraction for Data 3 is slightly lower than for Data 2. For the automatically processed images in Data 3, the K_{ax} is in fact lower than for Data 2. In short, rough tow boundaries are very effective in suppressing fluid velocity and thus artificially decrease permeability.

The effect of tow roughness on permeability is illustrated when the permeability results from Data 6 (Fig. 3D) and Data 7 (Fig. 3E) are compared. The images from Data 6 (Fig. 3D) are originally from Data 2 (Fig. 3A), the manually processed images. However, a small amount of random roughness was introduced in Data 6 while retaining nominally the same Brinkman fraction, leading to an increase in tow surface area. For Data 7, the images in Data 2 were dilated to increase the Brinkman fraction, but the roughness was not altered. When the axial K from Data 7 is compared to Data 6, the result is initially unexpected. A relative increase of roughly 4% of the Brinkman fraction in Data 7 should lead to a decrease in K_{ax} over Data 6, but the result is the opposite. The K_{ax} of Data 7 is higher than Data 6. This comparison between the permeabilities from Data 6 and Data 7 means that surface roughness is comparable to or more influential than Brinkman fraction in influencing permeability when changes of similar magnitude are compared. Further analysis of tow surface area as a measure of roughness and contour velocity profiles support this conclusion [20]. In order to preserve the Brinkman fraction while minimizing tow roughness, the automatically processed images were subjected to further post-processing which eliminates small “peninsulas” emanating from the surface of the tows and then fills in the remaining small “inlets” on the tow surface. The relative surface area of the resulting data, Data 8, is markedly closer to the surface area of the manually processed image (Data 2) as shown in Table 1. The resulting permeability from Data 8 is considered to have very good agreement with the experimental values. For the first time, the actual reinforcement microstructure was obtained rapidly and non-destructive, and the information was successfully used in a permeability prediction.

An example of using OCT for composite NDE is discussed below. OCT x - z cross-sectional images were collected from a selected region of impact damage from the composite. These images were reconstructed into a volumetric representation and re-sliced along the x - y plane at $650 \mu\text{m}$ (z -axis) from the surface, as seen in Fig. 4. The OCT images are 5.3 mm along the x -axis (wide) and 6.0 mm along the y -axis (long). Fig. 4A compares the OCT image to the corresponding LSCM image, Fig. 4B. Both images are displayed as log (intensity).

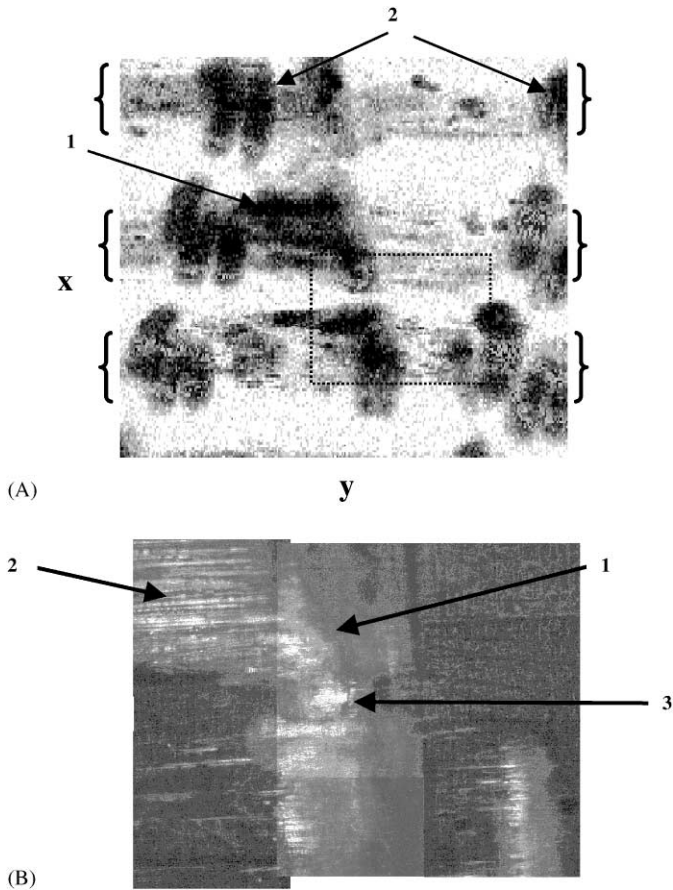


Fig. 4. OCT (A) and LSCM (B) images 650 μm from top surface of composite.

The damage seen by OCT is confirmed using LSCM. The OCT image in Fig. 4A shows the tows (bracketed sections) perpendicular and the crack parallel to the x -axis. The crack can be seen to run through 3 complete tow bundles (arrow 1). The stitching that holds each layer together is shown by arrow 2. The dashed square shows the area of the composite captured by confocal microscopy in Fig. 4B. The crack is still apparent (arrow 1) in Fig. 4B. Only the highly reflecting damage regions appear (arrow 2) with poor differentiation of tows. Both the LSCM and higher resolution OCT revealed the damage mechanism to be fiber de-bonding. The lower thickness resolution of the confocal is advantageous when features with diffuse boundaries are present, such as the cavitation region indicated by arrow 3. This cavitation is only partially seen in the OCT.

X-ray CT is a non-destructive characterization technique that is frequently used to image damage in composites [17,21]. Therefore, direct comparison of X-ray CT and OCT was deemed important. Fig. 5A displays the volumetric image of the impact

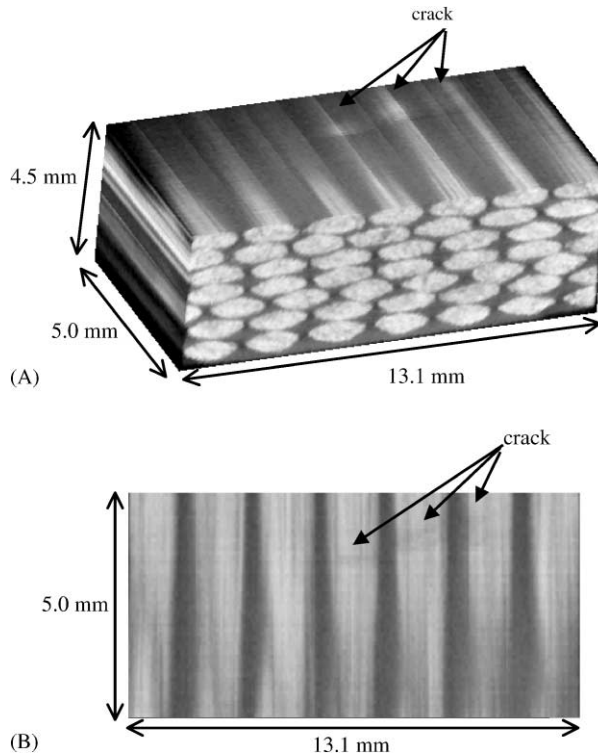


Fig. 5. X-ray CT images. Volumetric image showing entire sample with surface crack (A), x - y slice $650\ \mu\text{m}$ from the surface showing a faint crack across three glass tows as indicated by arrows (B).

damaged sample which is 13.1 mm along the x -axis, 4.5 mm along the z -axis, and 5 mm along the y -axis as defined in Fig. 2. The resolution of the image is $60\ \mu\text{m}$. From this figure, it is evident that X-ray CT does an excellent job at defining the preform architecture for the entire composite without any loss of contrast. However, the stitching used to hold the layers of glass tows together are transparent to the X-rays. This is because the difference in the electron density between the stitching and the epoxy resin is not enough to result in a X-ray attenuation difference of at least 0.1%–0.2% to generate contrast. Light areas at the surface of the composite are indicated by arrows in Fig. 5A. These areas are the clearest indications in the entire image that damage is present. The failure of X-ray CT to detect the damage is a reflection of the type of damage present. The Tactix and Jeffamine formulation results in a fairly tough resin matrix. With a tough matrix, the predominating failure modes are fiber de-bonding and cavitation. These failure modes do not result in sufficient attenuation differences to generate appreciable X-ray contrast. Fig. 5B shows a cross-sectional slice $650\ \mu\text{m}$ from the surface for comparison to Fig. 4. The damage seen in Fig. 4 is almost invisible to the X-rays and on the image, but is nevertheless indicated by arrows.

4. Conclusions

The microstructure of a unidirectional glass-reinforced composite was accurately and rapidly obtained using OCT. OCT images were processed and input into a microscale flow model for permeability prediction. It was found that the Brinkman fraction and tow surface area generated by the image processing have an important influence on the accuracy of the permeability calculations when compared to the expected values. By optimizing these effects during image processing, excellent agreement between the calculated and the experimental axial and transverse permeabilities was obtained.

Non-destructive evaluation of impact damage was compared using three techniques. The cracking and fiber de-bonding detected using OCT have been confirmed using confocal microscopy. The OCT images of the damage exhibited more detail and a higher depth of penetration than the LCSM. The OCT detected microstructural features as well as damage, whereas the LCSM only detected the damage. The LCSM performed better at detecting features with diffuse boundaries, like cavitation. X-ray CT did an excellent job of clearly imaging the reinforcement microstructure of the entire sample and was not limited in depth like the OCT. However, the type and extent of damage could not be elucidated using X-ray CT.

Acknowledgements

The authors gratefully acknowledge Dr. Mary McKnight of the NIST Building Materials Division for the generous use of her confocal microscope and helpful discussions.

References

- [1] Huang D, Swanson EA, Lin CP, Schuman JS, Stinson WG, Chang W, et al. Optical coherence tomography. *Science* 1991;254:1178–81.
- [2] Fujimoto JG, Brezinski ME, Tearney GJ, Boppart SA, Bouma B, Hee MR, et al. Optical biopsy and imaging using optical coherence tomography. *Nat Med* 1995;1:970–2.
- [3] Bashkansky M, Duncan MD, Kahn M, Lewis D, Reintjes J. Subsurface defect detection in ceramics by high-speed high-resolution optical coherent tomography. *Opt Lett* 1997;22:61.
- [4] Bouma B, Tearney GJ, Boppart SA, Hee MR, Brezinski ME, Fujimoto JG. High resolution optical coherence tomographic imaging using a modelocked Ti:Al₂O₃ laser source. *Opt Lett* 1995; 20:1–3.
- [5] Tearney GJ, Bouma BE, Boppart SA, Golubovic B, Swanson EA, Fujimoto JG. Rapid acquisition of in vivo biological images using optical coherence tomography. *Opt Lett* 1996;21:1408–10.
- [6] Parnas R, Salem A. A comparison of the unidirectional and radial in-plane flow of fluids through woven composite reinforcements. *Polymer Compos* 1993;14(5):383.
- [7] Friedman H, Johnson R, Miller B, Salem D, Parnas R. Forced in-plane flow through complex deformable structures: influence of an imposed curve. *Polymer Compos* 1997;18(5):663.
- [8] Ranganathan S, Wise G, Phelan Jr. F, Parnas R., Advani S. A numerical and experimental study of the permeability of fiber preforms. *Proceedings of the ACCE94, Dearborn, MI, 1994*, p. 309.

- [9] Phelan Jr. F, Wise G. Analysis of transverse flow in aligned fibrous porous media. *Composites: Part A* 1996;27A(1):25.
- [10] Spaid M, Phelan Jr. F. Lattice Boltzman methods for modeling microscale flow in porous media. *Phys Fluids* 1997;9(9):2468.
- [11] Spaid M, Phelan Jr. F. Modeling void formation dynamics in fibrous porous media with the lattice Boltzman method. *Composites: Part A* 1998;29:749.
- [12] Pitchumani R, Ramakrishnan B. A fractal geometry model for evaluating permeabilities of porous preforms used in liquid composite molding. *Int J Heat Mass Transfer* 1999;42(12):2219.
- [13] Ranganathan S, Easterling R, Advani S, Phelan Jr. F. The effect of microstructure variations on the permeability of preform material. *Polymers Polymer Compos* 1998;6(2):63.
- [14] Woo S, Daniel I. Three-dimensional ultrasonic imaging of defects and damage in composite materials. *Mater Eval* 1994;52(10):1199–206.
- [15] Dewhurst RJ, He R, Shan Q. Defect visualization in carbon fiber composite using laser ultrasound. *Mater Eval* 1993;51(8):935–40.
- [16] Highsmith AL, Keshav S. Quantitative assessment of fiber fracture in damaged laminates using x-ray radiography. *J Comp Tech Res* 1997;19(1):10–9.
- [17] Bossi RH, Georgeson GE. Composite structure development decisions using x-ray CT measurements. *Mater Eval* 1995;53(10):1198–203.
- [18] Izatt JA, Hee MR, Owen GM, Swanson EA, Fujimoto JG. Optical coherence microscopy in scattering media. *Opt Lett* 1994;19(8):590.
- [19] Dunkers J, Flynn K, Parnas R. A mid-infrared attenuated total internal reflection cure sensor for control of resin transfer molding of a pre-ceramic polymer. *Composites: Part A* 1997;28(2):163–70.
- [20] Dunkers J, Phelan F, Zimba C, Flynn K, Sanders D, Peterson R, et al. The prediction of permeability for an epoxy/E-glass composite using optical coherence tomographic images. *Phys Fluids*, in press.
- [21] Green WH, Sincebaugh P. Evaluation of complex composite structures using advanced computed tomography (CT) imaging. *Proceedings of The 53rd Meeting of the Society for Machinery Failure Prevention Technology*. Virginia Beach, VA, 1999. p. 41–50.